Article:
Fang, X., Peden, A.A., van Eeden, F.J.M. et al. (2021) Identification of additional outer segment targeting signals in zebrafish rod opsin. Journal of Cell Science, 134 (6). jcs.254995. ISSN: 0021-9533

https://doi.org/10.1242/jcs.254995

Identification of additional outer segment targeting signals in zebrafish rod opsin

Xiaoming Fang, Andrew A. Peden, Fredericus J.M. van Eeden*, Jarema J. Malicki

* author for correspondence

f.j.vaneeden@sheffield.ac.uk

University of Sheffield

Bateson Centre and the Department of Biomedical Science

Western Bank

Sheffield, S10 2TN

United Kingdom

Key words: Opsin, Cilia, GPCR, Photoreceptor, Vision

Summary statement

We identified a complex set of molecular features that function together as address labels to target opsin to the outer segment.

ABSTRACT

In vertebrate photoreceptors, opsins are highly concentrated in a morphologically distinct ciliary compartment known as the outer segment (OS). Opsin is synthesized in the cell body and transported to the OS at a remarkable rate of 100-1000 molecules per second. Opsin transport defects contribute to photoreceptor loss and blindness in human ciliopathies. Previous studies revealed that the opsin C-terminal tail, of 44 amino acids, is sufficient to mediate OS targeting in Xenopus photoreceptors. Here we show that although the Xenopus C-terminus retains this function in zebrafish, the homologous zebrafish sequence is not sufficient to target opsin to the OS. This functional difference is largely caused by a change of a single amino acid present in Xenopus, but not in other vertebrates examined. Furthermore, we find that sequences in the 3rd intracellular cytoplasmic loop (IC3) and adjacent regions of transmembrane helixes 6 and 7 are also necessary for opsin transport in zebrafish. Combined with the cytoplasmic tail, these sequences are sufficient to target opsin to the ciliary compartment.

Vertebrate photoreceptors detect light via a specialized cilium that contains hundreds of parallel membrane folds harboring the photosensitive pigment, opsin, and other components of the phototransduction cascade. It is estimated that 10^8-10^9 opsin molecules are tightly packed in the ciliary membranes of a single photoreceptor cell (Pugh and Lamb, 2000). Opsin is the main protein component of photoreceptor cilia and in addition to detecting light its presence is also essential for cilia morphogenesis (Lem et al., 1999, Pugh and Lamb, 2000). Photosensitive membranes of photoreceptors are continuously turned over: they are shed from the distal end of the cilium while new membrane folds are added to the cilium base (Young, 1967, Young and Droz, 1968). In the mouse retina, this process replaces approximately 10% of the photoreceptor ciliary membranes every day (LaVail, 1973). Consequently, 10% of all protein content of the cilium, including opsins and other phototransduction cascade components, are transported into the cilium every day.

The complex architecture of photosensitive membranes results in an unusually large volume of photoreceptor cilia (reviewed in ref.Kennedy and Malicki, 2009). The bulk of the cilium, referred to as the outer segment (OS), connects to the cell body via a narrow stalk, termed the connecting cilium, characterized by the typical architecture and dimensions of the ciliary transition zone (Tokuyasu and Yamada, 1959, Nilsson, 1964, Besharse et al., 1985, Röhlich, 1975). All proteins destined for the OS, including opsins, are transported through the connecting cilium (reviewed in Kennedy and Malicki, 2009, Malicki and Besharse, 2012). Given the unusually large size of the OS and its high protein content, transport into the photoreceptor cilium requires a particularly efficient mechanism (Malicki and Besharse, 2012).

Many attempts have been made to gain insight into the mechanism of rod opsin transport. A key finding in this area is that the cytoplasmic tail of 44 amino acids of rod opsin (hereafter CT44) is sufficient to mediate transport into the Xenopus OS (Tam et al., 2000). Human mutations in the homologous sequence lead to rapid vision loss (Sung et al., 1991, Bessant et al., 1999, Berson et al., 2002, reviewed in Athanasiou et al., 2018, Sung et al., 1994), which

further speaks to its importance. To direct transport, rod opsin C-terminal sequences must interact with protein components of cytoplasmic and/or ciliary transport machinery. Although some proteins that bind CT44 have been identified using biochemical approaches (Deretic et al., 2005, Mazelova et al., 2009, Wang et al., 2012, Tai et al., 1999, Chuang et al., 2007, Keady et al., 2011), the understanding of this process is far from complete. How such a functionally diverse group of proteins contributes to opsin transport requires further investigation. It is also noteworthy that based on previous analyses, opsin appeared to differ from other ciliary GPCRs, which contain a cilia targeting sequence (CTS) in the 3rd intracellular loop and do not display obvious homologies to opsin C-terminal targeting motifs (Berbari et al., 2008).

Here we further characterize rod opsin OS targeting. Surprisingly, we find that while Xenopus CT44 is sufficient to target an exogenous protein, such as GFP, to the ciliary compartment of zebrafish photoreceptors, the homologous zebrafish sequence is unable to do so. A single amino acid in the opsin helix 8 is predominantly responsible for this difference. This suggests that additional sequences are necessary to target rod opsins to the OS. Indeed, the analysis of Opsin/Sstr5 hybrid constructs reveals that a targeting sequence exists in the IC3 of rod opsin. Deletion of this motif causes opsin transport deficiency. Rod opsin ciliary targeting also requires parts of two transmembrane helixes that flank the 3rd cytoplasmic loop. These studies have uncovered novel motifs necessary to target rod opsin to the ciliary compartment of the photoreceptor in zebrafish and may allow for the identification of machinery involved in its transport in the future.

Results

Construction of transgenic tools to monitor opsin transport.

To monitor the dynamics of opsin transport in vivo, we generated stable zebrafish transgenic lines that express an EGFP-opsin fusion specifically in rod photoreceptors from an inducible

promoter. This system provides both spatial and temporal control of opsin expression. It consists of two transgenic lines: (1) A line that specifically expresses Cre recombinase in photoreceptors from the rhodopsin promoter, and (2) a temperature-inducible line that conditionally expresses EGFP-S-opsinCT44 (EGFP fused with S-peptide and Xenopus CT44) from a heat-shock promoter (Fig. 1A). A lox-mCherry-STOP-lox cassette is inserted upstream of EGFP-S-opsinCT44 in this line. When these two lines are crossed, Cre induces recombination specifically in rod photoreceptors, placing EGFP-S-opsinCT44 under the control of heat-shock promoter (Fig. 1A). When heat-shock is applied, embryos express EGFP-S-opsinCT44 specifically in rods and mCherry in all other cells (Fig. 1E). The EGFP-S-opsinCT44 fusion protein is efficiently transported to photoreceptor outer segments in these animals (Fig. 1E, I). In a control line, which contains 44 random amino acids in place of the 44 amino acids from rhodopsin C-terminus, the EGFP signal is no longer enriched in the OS and instead is present throughout the entire photoreceptor cytoplasm (Fig. 1F).

Zebrafish and Xenopus CT44 differ in their ability to opsin transport.

In Xenopus, CT44 is sufficient to mediate opsin OS targeting (Tam et al., 2000). To evaluate the function of the zebrafish opsin C-terminal region in OS-directed transport, we fused the 44 C-terminal amino acids of zebrafish rod opsin to EGFP and expressed it from a heat-shock promoter using stable transgenic lines, as previously described for Xenopus CT44 (Fig. 1). We compared EGFP transport efficiency in these lines to that in animals containing Xenopus CT44 transgene by assessing EGFP intensity in the cell body. We measured EGFP fluorescence in the cell body rather the OS, because the signal in the OS becomes saturated quickly, decreasing sensitivity of our measurements. Surprisingly, we found that in contrast to Xenopus C-terminus (XCT44), the equivalent region of zebrafish opsin (ZCT44) is very inefficient at targeting opsin to the zebrafish photoreceptor outer segment (Fig. 1G-I). Similar results were also obtained using a transient expression assay, in which we also used a heat-shock promoter to generate a pulse of GFP-CT44 expression and monitor the rate at which

opsin-GFP is cleared from the photoreceptor cell body (Zhao and Malicki, 2011) (Fig. 2B-D). These results indicate that, unexpectedly, opsin targeting mechanisms differ significantly among vertebrate species.

The 44 C-terminal amino acids of opsin sequence contain an α-helical region, referred to as the helix 8, flanked on the C-terminal side by a pair of cysteines (Fig. 2A) (Palczewski et al., 2000). Several studies suggested that helix 8 mediates opsin dimerization, which, in turn, may play a role in opsin transport (Knepp et al., 2012, Zhang et al., 2016). We therefore hypothesized that helix 8 is responsible for differences in opsin transport efficiency between zebrafish (ZCT44) and Xenopus (XCT44) C-terminal regions. To test this, we replaced helix 8 in the zebrafish C-terminal cytoplasmic tail with the Xenopus sequence (Fig. 2E) and vice versa, we substituted helix 8 of the Xenopus C-terminal tail with the zebrafish sequence (Fig. 2F). The Xenopus helix 8 very significantly improved transport efficiency of ZCT44 (Fig. 2E, I, $p < 0.001$). Consistent with that, replacing Xenopus CT44 helix 8 with the zebrafish sequence strongly decreased targeting efficiency (Fig. 2F, I, $p<0.001$). Xenopus sequences outside helix 8 affect opsin targeting to a lesser degree: replacing the C-terminal sequence of zebrafish ZCT44 with the Xenopus sequence does not result in a significant difference (compare D to F, and I). Replacing the same fragment of Xenopus CT44 with the zebrafish sequence does, however, somewhat decrease targeting efficiency (Fig. 2E, I, $p < 0.05$). These results demonstrate that helix 8 is of paramount importance for the OS targeting of opsin.

Rod opsin helix 8 is very well conserved across vertebrate phyla (Fig. S1). Zebrafish and Xenopus helix 8 sequences differ only at two positions: 315 and 317 (Fig. 2A). To narrow down which amino acid contributes to opsin targeting efficiency the most, we substituted single amino acids in zebrafish helix 8 with Xenopus ones. We found that while H315N substitution alters transport relatively weakly ($p <0.05$) (Fig. 2G, I), the substitution of methionine 317 with leucine (M317L) significantly improves transport efficiency (Fig. 2H, I, $p < 0.01$). Sequence comparison of rod opsins from over 20 vertebrate species reveals that position 317 is almost

invariably occupied by methionine (Fig S1). The sole exception among these species is Xenopus. To test whether the exceptional targeting ability of XCT44 is due to the presence of the leucine, we introduced the sequence of human rod opsin C-terminus (HCT38) to the transient assay. In line with the zebrafish CT44, the targeting deficiency of human CT38, compared to Xenopus CT44, was significantly improved by its M317L substitution (Fig. S2B-D, G). We were curious how Leu317 would behave in non-opsin GPCRs. To address this question, we replaced the entire helix 8 in XCT44 with the C-terminal sequence of porcine α adrenergic receptor (Standfuss et al., 2011), which is a GPCR that shares structural similarities with rod opsin. This chimera, which is supposed to localize to the Xenopus outer segment (Tam et al., 2000), was found mainly in the cell body and the synapse of zebrafish photoreceptors. Strikingly, the substitution of phenylalanine with leucine also enhanced the OS targeting to a significant level (Fig. S2E-G). Given the importance of this amino acid in opsin targeting (Fig. 2I), our findings show that Xenopus CT44 transport into the outer segment is mediated by different molecular interactions, compared to that of zebrafish CT44, and highly likely compared to most other vertebrate rod opsins. Importantly, these findings reveal that in addition to the opsin C-terminus, other opsin sequences are necessary to target opsin to the outer segment.

Additional opsin ciliary targeting motifs

To search for additional OS-targeting signals in the opsin sequence, we constructed a series of hybrid GPCRs combining sequences from zebrafish rod opsin and another GPCR, Sstr5. We chose Sstr5 because unlike its close relative, SSTR3, it is not targeted to cilia (Berbari et al., 2008). All constructs were transiently expressed from a heat-shock promoter as above. Compared to opsin, Sstr5 is transported to the photoreceptor ciliary outer segment very inefficiently (Fig. 3A, B; compare constructs no. 1 and 2). Substitution of Sstr5 C-terminal cytoplasmic tail with zebrafish CT44 did not result in a significant improvement of transport efficiency (construct no. 3, Fig. 3A, B). The deficiency was preserved when we replaced the

Sstr5 sequence with a non-OS-targeted photopigment, melanopsin (Opn4a), sequence (Matos-Cruz et al., 2011, Davies et al., 2011) (Fig. S3A, B). Analysis of 4 additional hybrid constructs revealed that transport efficiency correlates with the presence of IC3, which is the equivalent region where several other GPCRs' ciliary targeting motifs are also found (Berbari et al., 2008, Loktev and Jackson, 2013, Nagata et al., 2013) (Fig. 3A, B; constructs 4 - 7). Consistently, replacement of this loop with the Sstr5 sequence resulted in a dramatic loss of transport efficiency (Fig. 3A, B; compare no. 2 to 8). These studies show that IC3 is required for opsin targeting to the OS.

The assay that we use to monitor opsin transport efficiency into the ciliary compartment measures the rate of GFP signal loss in the photoreceptor cell body. In addition to OS-directed transport, loss of GFP signal could be caused, however, by degradation of opsin/Sstr5-GFP hybrid polypeptides in the cell body. To test this, we expressed four hybrid constructs: two that are efficiently transported to the ciliary outer segment (no. 4 and no. 6) and two that are not (no. 5 and no. 8) in photoreceptors of *oval* (*ovl*) mutants. We showed previously that ovl^{tz288b} strain harbors a mutation in the *ift88* gene that causes complete loss of the photoreceptor outer segment (Tsujikawa and Malicki, 2004). In the absence of the outer segment, opsin/Sstr5-GFP hybrids remain trapped in the cell body (Fig. 3C). We compared cytoplasmic expression levels of opsin/Sstr5-GFP hybrid constructs at 5 and 12h post heat shock. We did not see statistically significant loss of GFP signal for any of the fusion constructs tested (Fig. 3D). Some signal loss between 5 and 12h, albeit not statistically significant, was seen for no. 8. For hybrid no. 6, a small but statistically significant increase of signal was observed. These findings indicate that degradation is not a factor that significantly contributes to the rate of signal loss from the photoreceptor cell body in our assay. Moreover, we did not observe a relationship between the overall expression level and the rate of GFP signal loss from the cell body: although fusion no. 8 was expressed at a higher level compared to other constructs, no. 5 was not and yet it was inefficiently transported to the outer segment (Fig. 3D). Finally, we did not see a statistically significant photoreceptor cell loss

for any construct between 5 and 12 hours post heat-shock (Fig. S3E). Cell loss is thus unlikely to account for differences in cell body GFP signal level. Taken together, these findings reveal that opsin transport into the outer segment requires a targeting sequence in the IC3 of opsin.

To define sequences sufficient to mediate outer segment transport, we inserted opsin IC3 and CT44 into Sstr5 (construct no. 9) (Fig. 4). This hybrid GPCR fails to localize to the outer segment, indicating that these two fragments of opsin sequence are not sufficient to target opsin to the OS. Similarly, a hybrid, that in addition to IC3 and CT44, contains helix 6 from opsin (Fig. 4A, C; no. 11) is not efficiently targeted to the OS and substitution of opsin helix 6 in hybrid no. 6 with the Sstr5 sequence (Fig. 4A; hybrid no. 13) also impairs targeting to the ciliary compartment (Fig. 4C). These results suggest that rod opsin transport mechanism involves both helixes 6 and 7. Coherently, based on the opsin crystal structure (Park et al., 2008, Palczewski et al., 2000), these helixes are close to each other and may interact to maintain opsin conformation and the relative positions of IC3 and CT44. To narrow down which parts of helix 6 and 7 are required for the ciliary targeting of opsin, we constructed a hybrid containing the N-terminal half of helix 6 and the C-terminal half of helix 7 from rod opsin in addition to opsin IC3 and CT44 (Fig. 4A, no. 14). We found that this configuration of opsin sequences is sufficient to mediate outer segment targeting with the same efficiency as the full-length sequence (Fig. 4C).

Studies of SSTR3 identified a conserved motif in IC3 as necessary for ciliary targeting (Berbari et al., 2008). To test whether it is also required for opsin targeting, we deleted this motif (AAAQQQ) from the full length rod opsin (construct no. 12, Fig. 4B). In contrast to SSTR3, this deletion does not affect OS targeting in photoreceptors (Fig. 4D). Thus, we were interested in which particular motif within IC3 is essential for its role in regard to OS targeting, as the common ciliary targeting motif appeared to be redundant for transport. To address this question, two additional deletion constructs (Fig. 4B and D; no. 16 and no. 17) were tested and the OS targeting defect was only observed in the absence of RAERE sequence, which is

adjacent to helix 6, but the ESETTQ motif had no effect on opsin transport. It is possible, that the defect in OS targeting observed in the RAERE mutant could simply be explained by a defect in protein folding and transport. To address this, we expressed these opsin variants in PAC2 cells and visualized their localization. All of the above opsin variants are able to escape from the endoplasmic reticulum (ER) and reach the plasma membrane as the full-length opsin (Fig. S4), suggesting that their mislocalization was not due to protein misfolding and ER retention. Taken together, these results define CT44, IC3 and parts of helixes 6 and 7 as both necessary and sufficient to target opsin to the ciliary outer segment in vertebrate photoreceptors.

Discussion

Cilia-targeting sequences have been identified for several proteins, including Polycystins, CNG channel, INPP5E and several GPCRs, including opsin (reviewed in Malicki and Avidor-Reiss, 2014). However, there does not appear to be a common ciliary targeting motif. GPCRs are to be thought to be transported to cilia by multiple mechanisms: while the C-terminal cytoplasmic tail appeared sufficient for opsin targeting to the OS, entirely different targeting motifs in the third cytoplasmic loop were shown to target other GPCRs to the ciliary compartment (Loktev and Jackson, 2013, Mukhopadhyay et al., 2013, Berbari et al., 2008). Targeting motifs found in other GPCRs appeared irrelevant to opsin because the opsin cytoplasmic tail seemed sufficient to target Xenopus opsin to the ciliary compartment (Tam et al., 2000). Conversely, opsin C-terminal targeting motifs, such as VxPx, are poorly conserved in SSTRs, if at all, supporting the idea that opsins utilize different targeting mechanisms, compared to other GPCRs. In addition, the VxPx motif was shown to have negative effects on primary cilia targeting (Geneva et al., 2017), suggesting distinct transport mechanisms act in different cell types. Our data establish, however, that in our model system the third intracellular loop of opsin is essential for the targeting towards photoreceptor ciliary compartments, implying that at least some aspects of opsin transport are closely related to those of other GPCRs.

The (AX[S/A]XQ) motif, previously identified in other GPCRs and conserved in the opsin sequence, is not, however, necessary for opsin transport in our assay. This is not entirely unexpected as ciliary targeting motifs in the IC3 of GPCRs vary substantially: the [R/K][I/L]W motif of NPY2R and [I/V]KARK of GPR161 are not related to the ciliary targeting sequence of SSTR3 and do not display clear similarity to each other apart from the presence of basic and hydrophobic residues (Mukhopadhyay et al., 2013, Loktev and Jackson, 2013). In addition, in agreement with our analysis, mutating the SSTR3-related motif does not affect the ciliary trafficking of GPR83 (Loktev and Jackson, 2013). Rod opsin is thus likely to have yet another set of targeting motifs in IC3. Indeed, our data suggests that the RAERE motif in the IC3 is necessary for opsin OS targeting. Work of several groups' has shed the light on proteins that facilitate opsin transport, including Arf4 (Deretic et al., 2005, Mazelova et al., 2009), ASAP1, Rab8 and Rab11 (Wang et al., 2012) and IFTs (Keady et al., 2011, Crouse et al., 2014). It has been shown that Arf4 binds to the VxPx motif and ASAP1 binds to the FR motif at the opsin C termini (Fig. 5E). However, some of these components appear to be dispensable in vivo for opsin transport (Pearring et al., 2017, Ying et al., 2016). Our data suggests the IC3 potentially could be a new binding site for trafficking machinery. The IC3 was suggested as a binding site for TULP3 and RABL2, which have been shown to act as adaptors (Barbeito et al., 2020, Badgandi et al., 2017) for transport of several GPCRs to the primary cilium. In the future, the role of IC3 as an interacting site for opsin transport will need to be further addressed by biochemical approaches.

Our studies show that in addition to targeting motifs in the third intracellular loop, parts of helixes 6 and 7 on the intracellular side of the membrane also contribute to opsin transport (summarized in Fig. 5). In crystal structures (Palczewski et al., 2000, Park et al., 2008), these helixes localize close to each other (Fig. 5B-D) and their interactions may be necessary to position IC3 and/or helix 8 in a way that facilitates interactions with components of the ciliary transport machinery (Fig. 5E). Interestingly, both helix 6 and helix 7 contain residues

(Met253, Met257, Ile305 and others Fig. 5D), that are well conserved among ciliary but not rhabdomeric opsins (Arendt et al., 2004), supporting the conclusion that these helixes are involved in OS targeting. Additionally, we show that segments of both helixes are required to facilitate efficient OS targeting, consistent with the hypothesis that their interaction with each other is required.

A surprising conclusion of our analysis is that Xenopus C-terminal sequence functions as an OS targeting signal in zebrafish photoreceptors while the homologous zebrafish sequence does not. The alignment of opsins from vertebrates (Fig. S1) shows that Met317 is conserved in all species examined, except Xenopus, where it is substituted by leucine. This suggests that Xenopus opsin transport may be different from other vertebrates. Interestingly, we also observed that the human sequence and its leucine variant behave in the same way as the zebrafish constructs (Fig. S2B-D). At present it is unclear why the leucine substitution could make such dramatic changes for OS targeting.

One possibility is that the Xenopus C-terminal tail has unusually strong propensity to bind components of opsin transport machinery, whereas additional sequences are required for zebrafish and other opsins to achieve sufficient interactions. This would explain why Xenopus CT44 is efficiently targeted to the outer segment in zebrafish, but the homologous sequence from zebrafish does not behave in this way. Xenopus opsin transport may need to be significantly more efficient because the Xenopus rod OS is ~30 fold larger than the mouse rod OS. In addition, the replenishment rate of the OS is higher in Xenopus (~8 fold higher than in the mouse) compared to other species (Pearring et al., 2013).

An additional explanation for the ability of the Xenopus opsin C terminus to more efficiently target to the OS may be linked to the likelihood of opsin dimer formation. Several lines of evidence show that helix 8 together with helix 1 form one of the possible interfaces that mediate interactions between opsin molecules. First, an opsin homodimer crystal structure (PBD ID

3CAP) shows that helixes 8 and 1 are positioned at the dimerization interface (Park et al., 2008). Second, chemical cross-linking in bovine rod outer segment membranes identified a Cys316-Cys316 cross link between helixes 8 of two monomers (Knepp et al., 2012), again suggesting that helix 8 mediates dimerization. Notably, Cys316 is adjacent to Leu317 that we identified as essential for efficient XCT44 targeting to the OS. Finally, delivery of helix 8 peptide to mouse photoreceptors mislocalizes opsin, most likely due to interference with dimerization (Zhang et al., 2016). The alignment of opsins from vertebrates (Fig. S1) shows that Met317 is conserved in all species examined, except Xenopus, where it is substituted by leucine. This reveals that Xenopus opsin transport involves molecular features not shared with other vertebrates. In the light of evidence that helix 8 mediates opsin dimerization, an intriguing possibility is that the Xenopus C-terminal tail has unusually strong propensity to dimerize and consequently is co-transported, or "hitch-hikes," with the full-length wild-type protein. This would explain why Xenopus CT44 is efficiently targeted to the outer segment in zebrafish, but the homologous sequence from zebrafish does not behave in this way. A caveat is that multiple intradimeric contacts, including helix 1 and 2, 1and 5, 1 and 8, 4 and 5 etc., have been identified by studies using electron microscopy, atomic force microscopy as well as biochemical tools (Knepp et al., 2012, Jastrzebska et al., 2015, Liang et al., 2003, Ploier et al., 2016, Salom et al., 2006). Thus, whether opsin transport is in the form of dimer/oligomer, and whether helix 8 participates in, or is sufficient for, dimerization, are questions that remain to be addressed.

It is also possible that zebrafish opsin transport is different to that of higher vertebrates. For example, the zebrafish C-terminal sequence does not function well on its own or fused to the transmembrane domain of other GPCRs. However, the mouse rod opsin C-terminal sequence is able to direct part of peripherin, which lacks the C-terminal targeting signal, to the OS (Salinas et al., 2017, Tam et al., 2004, Salinas et al., 2013). At present, no study has directly tested how an isolated C-terminus behaves in mouse photoreceptors. However, it is worth noting that the RAERE motif is conserved in higher vertebrates as KAEKE and it is commonly

shared within ciliary opsins but not within rhabdomeric opsins (Arendt et al., 2004). In the future, it will be important to directly test whether these residues are critical for opsin transport in higher vertebrates and if they play a role in binding transport machinery.

Materials and Methods

Zebrafish strains and maintenance

Zebrafish were maintained in the University of Sheffield aquarium facility in accordance with UK Home Office requirements. Embryos of AB, LWT (London Wild-type) or Nacre lines were used for transient expression assays and transgenesis. The *ovl*^{tz288b} strain was described by us previously (Tsujikawa and Malicki, 2004).

DNA constructs

Two transgenes were used to obtain spatial and temporal control of expression in photoreceptor cells: the Cre expression transgene, and a conditional EGFP-CT44 transgene. To obtain rod specific Cre expression, we cloned the 1.3 kb BglII-BamHI fragment from the XopsEGFP-N1 plasmid (Fadool, 2003), containing the Xenopus rod opsin promoter, into the p5E-MCS vector. The resulting entry clone: p5E-XOPS-1324, pME-Cre, and p3E-PolyA, were assembled into a pDestTol2CG2 destination vector, using Gateway reaction as described (Kwan et al., 2007). To construct conditional EGFP-S-CT44 transgenes, we synthesized a DNA fragment encoding a C-terminal fragment of EGFP fused to a 2xTEV-S-tag-CT44-polyA sequence (Integrated DNA Technologies, IDT) and combined it by overlap extension PCR with a lox2272-EGFP sequence. The PCR amplification product was inserted into the Gateway entry vector p3E-MCS (Invitrogen, Inc.). The resulting entry clone was combined with p5E-hsp70 (Kwan et al., 2007), and pME-lox2272-mCherry(stop) in the pDestTol2pA2 destination vector, using the Gateway reaction. Three versions of the conditional EGFP-CT44 transgene were made, containing zebrafish CT44 (CT44), Xenopus CT44 (XCT44), or a random 44 amino acid control sequence (CTC). The transgenes are termed as follows:

Tg(XOPS-1324:Cre),
Tg(hsp70: lox2272-mCherry-lox2272-EGFP-2xTEV-S-tag-XCT44),
Tg(hsp70: lox2272-mCherry-lox2272-EGFP-2xTEV-S-tag-ZCT44),
Tg(hsp70:lox2272-mCherry-lox2272-EGFP-2xTEV-S-tag-CTC)

To test zebrafish and Xenopus CT44 cilia targeting sequences in transient expression assays, we first inserted EGFP between HindIII and EcoRI sites in the pME-MCS Gateway vector from the zebrafish Tol2 transgenesis kit (Kwan et al., 2007). The zebrafish CT44 sequence was then inserted downstream of EGFP between EcoRI and BamHI sites. The heat-shock promoter and the polyA site were added using p5E-hsp70 and p3E-polyA entry clones from the same kit. We used a Gateway reaction to assemble the entry clones into the pDestTol2-CG2 destination vector, which includes *cmlc2:eGFP* as a transgenesis marker. Zebrafish/Xenopus hybrid CT44 sequences were assembled by PCR using forward primers encoding Xenopus or Zebrafish Helix 8 or their mutant variants (Fig. 2). Zebrafish or Xenopus CT44 sequence was used as a template. Human constructs, AAR and their variants were made following the above strategy. Human and AAR sequences were obtained through DNA synthesis.

For opsin/Sstr5 hybrid experiments, the opsin reference construct was prepared by inserting EGFP after T336 in the ASTTASK sequence in zebrafish rod opsin (UniProtKB - P35359). An additional serine was introduced in this process generating the following insertion: AST-(EGFP)-STASK. This resulted in a fusion similar to that previously used to test bovine opsin transport (Moritz et al., 2001). The sstr5 reference construct was generated by appending EGFP to the C-terminus of the zebrafish sstr5 sequence (UniProtKB - Q6NV10), which was amplified from zebrafish cDNA. The melanopsin reference construct was cloned using the same procedure as for sstr5 one. The zebrafish melanopsin gene (Gene ID: 571624) was amplified from a cDNA clone (Source Bioscience, IRCYp5023J172D). Opsin-EGFP, Sstr5-EGFP and melanopsin-EGFP constructs were inserted into EcoRI/BamHI (opsin), HindIII/BamHI (sstr5) or XhoI/NotI (melanopsin) sites of the pME-MCS vector. All

opsin/sstr5 and opsin/melanopsin hybrid constructs were made by overlap extension PCR and inserted into either EcoRI/BamHI (No5, 8, 12, 16, 17) or HindIII/BamHI (No3, 4, 6, 7, 9, 11, 13, 14) or XhoI/BamHI (ML-No3) sites of the same vector. To generate the final heat shock promoter expression constructs, three entry clones, p5E-hsp70, pME-opsin/sstr5 and p3E-polyA were combined as above. The structure of all final constructs was confirmed by sequencing. Full amino acid sequences of opsin/Sstr5 and opsin/melanopsin are listed in supplementary Table S1.

Embryo Injections and Transgenesis

To generate stable transgenic lines and to perform transient expression assays, constructs were microinjected with Tol2 transposase as described (Kwan et al., 2007). While performing transient expression assays, in each experiment all constructs analyzed were injected during a single session. To obtain stable transgenic lines, XOPS-1324-Cre transgenic fish were selected at 3 dpf on the basis of cmlc:GFP expression. To generate fish transgenic for conditional EGFP-S-CT44 constructs, G0 larvae were screened 3-4 days after injection by heat shocking and selecting for mCherry expression 8 hours post heat shock, using a high power fluorescence dissecting microscope. The same procedure was used in the F1 generation and mCherry-positive fish were raised to adulthood. Single transgene insertions that segregate in a Mendelian fashion were identified in subsequent generations.

Transient expression assays

In transient expression assays, four-day wild-type larvae were heat-shocked at 39^{O}C for 30 (CT44 analysis) or 10 (opsin/Sstr5 assays) or 20 min. (opsin/melanopsin). Larvae with GFP-positive hearts were selected 5-6 h after heat shock and fixed 24h post heat shock. Fixation, cryosectioning and imaging was performed as described (Malicki et al., 2016). Prior to imaging, sections were counterstained for 10 min. in DAPI solution. For analysis in *ovl*$^{-/-}$ mutant background, opsin/sstr5 hybrid constructs were injected into embryos originating from

a *ovl*$^{+/-}$ heterozygotes cross. Homozygous mutants were heat shocked at 3 dpf for 10 min. and fixed 5 or 12 hours post heat shock.

Assays using stable transgenic lines.

For the analysis of opsin transport in wild-type retinae, single or double transgenics were heat shocked at 4 dpf for 30 (EGFP-ZCT44) or 5 (EGFP-XCT44) minutes and analyzed at 5 hr and 24 hr post heat shock. Different heat shock times were used to compensate for the difference in the expression level of ZCT44 and XCT44 transgenes due to positional effects of transgene insertion. mCherry-positive larvae with green hearts were selected and processed for cryosectioning as above.

Image analysis

Single optical sections in the plane of retinal cryosections were acquired on an Olympus FV1000 Confocal microscope and saved as .oif format files, which were then processed using Fiji software. Signal intensity from the GFP channel was color-coded using a thermal lookup table. To measure signal intensity in photoreceptor cell bodies, a line, approximately 2.5 μm wide, was drawn from the synapse to the outer segment base for each GFP-positive photoreceptor using Fiji software. Mean signal intensity in the area covered by the line was quantified and the resulting images were flattened and stored as TIFF files. To avoid signal overlap from neighboring cells, isolated GFP-positive cells were preferred for this analysis.

Statistical Analysis

To analyze cytoplasmic GFP intensity in stable transgenic lines (Fig. 1), we log transformed signal intensity data and analyzed them using 2-way ANOVA. Similarly, all other GFP intensity data were log transformed. The resulting data sets approximated normal distribution and were analyzed using ANOVA of mixed effects models assuming fish as a random effect. Mann-Whitney test was used for data sets containing signal intensity, which was averaged per animal. * < 0.05; ** < 0.01; *** < 0.001; **** <0.0001.

Cell culture and immunofluorescence

PAC2 cells (Martin Lowe, University of Manchester, UK) were cultured at 28 ^{O}C with 0.1% CO_2 and L-15 medium containing 10% FBS and 1% Penicillin/Streptomycin. Transfections were performed according to the manufacturer's protocol for FuGENE HD transfection reagent (Promega E2311). Heatshock was applied 4 hours post transfection at 39 ^{O}C and cells were fixed by 4% PFA/PBS 48 hours after heatshock followed by 0.1% Triton X-100/PBS permeabilization. Permeabilization was not applied if followed by 4D2 staining. 1% BSA/PBS was used for blocking and cells were stained by the following antibodies: anti-GRP78/Bip (Eames et al., 2013) (1:200, Abcam), anti-Rhodopsin Rho-4D2 (Salinas et al., 2017) (1:100, Abcam) and Alexa Fluor 568 anti mouse or rabbit conjugated secondary antibody (1:500, Invitrogen). Anti-GRP78/Bip antibody was applied to label the ER. Anti-Rho-4D2 antibody recognizes the N terminus of rod opsin. Without permeabilization, anti-Rho-4D2 only detects opsin molecules that reach the plasma membrane.

Acknowledgements We thank Vadim Arshavsky, Elizabeth Smythe, Michael Cheetham, Ryan MacDonald, Stone Elworthy, Anton Nikolaev, Seth Blackshaw, Eleanor Markham and Daniel Williams for helpful comments on earlier versions of this work. Amy Spencer from the Statistical Services Unit helped with data analysis. Martin Lowe for providing PAC2 cell line.

Funding

This work was supported by Fight for Sight UK (1856/1857 to J.J.M), Medical Research Council (MR/N000714/1 to J.J.M) and Biotechnology and Biological Sciences Research Council (BB/R005192/1 to J.J.M)

Conflict of Interest Statement

The authors declare no conflict of interest.

Data Availability

All data are made available in the paper.

References

ARENDT, D., TESSMAR-RAIBLE, K., SNYMAN, H., DORRESTEIJN, A. W. & WITTBRODT, J. 2004. Ciliary photoreceptors with a vertebrate-type opsin in an invertebrate brain. *Science,* 306**,** 869-871.

ATHANASIOU, D., AGUILA, M., BELLINGHAM, J., LI, W., MCCULLEY, C., REEVES, P. J. & CHEETHAM, M. E. 2018. The molecular and cellular basis of rhodopsin retinitis pigmentosa reveals potential strategies for therapy. *Progress in retinal and eye research,* 62**,** 1-23.

BADGANDI, H. B., HWANG, S.-H., SHIMADA, I. S., LORIOT, E. & MUKHOPADHYAY, S. 2017. Tubby family proteins are adapters for ciliary trafficking of integral membrane proteins. *J Cell Biol***,** jcb. 201607095.

BARBEITO, P., TACHIBANA, Y., MARTIN-MORALES, R., MORENO, P., MYKYTYN, K., KOBAYASHI, T. & GARCIA-GONZALO, F. R. 2020. HTR6 and SSTR3 ciliary targeting relies on both IC3 loops and C-terminal tails. *Life Science Alliance,* 4**,** e202000746.

BERBARI, N. F., JOHNSON, A. D., LEWIS, J. S., ASKWITH, C. C. & MYKYTYN, K. 2008. Identification of ciliary localization sequences within the third intracellular loop of G protein-coupled receptors. *Molecular biology of the cell,* 19**,** 1540-1547.

BERSON, E. L., ROSNER, B., WEIGEL-DIFRANCO, C., DRYJA, T. P. & SANDBERG, M. A. 2002. Disease progression in patients with dominant retinitis pigmentosa and rhodopsin mutations. *Invest Ophthalmol Vis Sci,* 43**,** 3027-36.

BESHARSE, J. C., FORESTNER, D. M. & DEFOE, D. M. 1985. Membrane assembly in retinal photoreceptors. III. Distinct membrane domains of the connecting cilium of developing rods. *The Journal of neuroscience,* 5**,** 1035-48.

BESSANT, D. A., KHALIQ, S., HAMEED, A., ANWAR, K., PAYNE, A. M., MEHDI, S. Q. & BHATTACHARYA, S. S. 1999. Severe autosomal dominant retinitis pigmentosa caused by a novel rhodopsin mutation (Ter349Glu). Mutations in brief no. 208. Online. *Hum Mutat,* 13**,** 83.

CHUANG, J. Z., ZHAO, Y. & SUNG, C. H. 2007. SARA-regulated vesicular targeting underlies formation of the light-sensing organelle in mammalian rods. *Cell,* 130**,** 535-47.

CROUSE, J. A., LOPES, V. S., SANAGUSTIN, J. T., KEADY, B. T., WILLIAMS, D. S. & PAZOUR, G. J. 2014. Distinct functions for IFT140 and IFT20 in opsin transport. *Cytoskeleton,* 71**,** 302-310.

DAVIES, W. I., ZHENG, L., HUGHES, S., TAMAI, T. K., TURTON, M., HALFORD, S., FOSTER, R. G., WHITMORE, D. & HANKINS, M. W. 2011. Functional diversity of melanopsins and their global expression in the teleost retina. *Cellular and Molecular Life Sciences,* 68**,** 4115-4132.

DERETIC, D., WILLIAMS, A. H., RANSOM, N., MOREL, V., HARGRAVE, P. A. & ARENDT, A. 2005. Rhodopsin C terminus, the site of mutations causing retinal disease, regulates trafficking by binding to ADP-ribosylation factor 4 (ARF4). *Proceedings of the National Academy of Sciences,* 102**,** 3301-3306.

EAMES, S. C., KINKEL, M. D., RAJAN, S., PRINCE, V. E. & PHILIPSON, L. H. 2013. Transgenic

zebrafish model of the C43G human insulin gene mutation. *Journal of diabetes investigation,* 4**,** 157-167.

FADOOL, J. M. 2003. Development of a rod photoreceptor mosaic revealed in transgenic zebrafish. *Dev Biol,* 258**,** 277-90.

GENEVA, I. I., TAN, H. Y. & CALVERT, P. D. 2017. Untangling ciliary access and enrichment of two rhodopsin-like receptors using quantitative fluorescence microscopy reveals cell-specific sorting pathways. *Molecular biology of the cell,* 28**,** 554-566.

JASTRZEBSKA, B., CHEN, Y., ORBAN, T., JIN, H., HOFMANN, L. & PALCZEWSKI, K. 2015. Disruption of rhodopsin dimerization with synthetic peptides targeting an interaction interface. *Journal of Biological Chemistry,* 290**,** 25728-25744.

KEADY, B. T., LE, Y. Z. & PAZOUR, G. J. 2011. IFT20 is required for opsin trafficking and photoreceptor outer segment development. *Molecular biology of the cell,* 22**,** 921-930.

KENNEDY, B. & MALICKI, J. 2009. What drives cell morphogenesis: a look inside the vertebrate photoreceptor. *Dev Dyn,* 238**,** 2115-38.

KNEPP, A. M., PERIOLE, X., MARRINK, S.-J., SAKMAR, T. P. & HUBER, T. 2012. Rhodopsin forms a dimer with cytoplasmic helix 8 contacts in native membranes. *Biochemistry,* 51**,** 1819-1821.

KWAN, K. M., FUJIMOTO, E., GRABHER, C., MANGUM, B. D., HARDY, M. E., CAMPBELL, D. S., PARANT, J. M., YOST, H. J., KANKI, J. P. & CHIEN, C. B. 2007. The Tol2kit: a multisite gateway-based construction kit for Tol2 transposon transgenesis constructs. *Dev Dyn,* 236**,** 3088-99.

LAVAIL, M. M. 1973. Kinetics of rod outer segment renewal in the developing mouse retina. *The Journal of cell biology,* 58**,** 650-61.

LEM, J., KRASNOPEROVA, N. V., CALVERT, P. D., KOSARAS, B., CAMERON, D. A., NICOLO, M., MAKINO, C. L. & SIDMAN, R. L. 1999. Morphological, physiological, and biochemical changes in rhodopsin knockout mice. *PNAS,* 96**,** 736-41.

LIANG, Y., FOTIADIS, D., FILIPEK, S., SAPERSTEIN, D. A., PALCZEWSKI, K. & ENGEL, A. 2003. Organization of the G protein-coupled receptors rhodopsin and opsin in native membranes. *Journal of Biological Chemistry,* 278**,** 21655-21662.

LOKTEV, A. V. & JACKSON, P. K. 2013. Neuropeptide Y family receptors traffic via the Bardet-Biedl syndrome pathway to signal in neuronal primary cilia. *Cell reports,* 5**,** 1316-1329.

MALICKI, J. & AVIDOR-REISS, T. 2014. From the cytoplasm into the cilium: bon voyage. *Organogenesis,* 10**,** 138-57.

MALICKI, J. & BESHARSE, J. C. 2012. Kinesin-2 family motors in the unusual photoreceptor cilium. *Vision Research,* 75**,** 33-36.

MALICKI, J., POORANACHANDRAN, N., NIKOLAEV, A., FANG, X. & AVANESOV, A. 2016. Analysis of the retina in the zebrafish model. *Methods Cell Biol,* 134**,** 257-334.

MATOS-CRUZ, V., BLASIC, J., NICKLE, B., ROBINSON, P. R., HATTAR, S. & HALPERN, M. E. 2011. Unexpected diversity and photoperiod dependence of the zebrafish melanopsin system. *PloS one,* 6**,** e25111.

MAZELOVA, J., ASTUTO-GRIBBLE, L., INOUE, H., TAM, B. M., SCHONTEICH, E., PREKERIS,

R., MORITZ, O. L., RANDAZZO, P. A. & DERETIC, D. 2009. Ciliary targeting motif VxPx directs assembly of a trafficking module through Arf4. *EMBO J,* 28**,** 183-92.

MUKHOPADHYAY, S., WEN, X., RATTI, N., LOKTEV, A., RANGELL, L., SCALES, S. J. & JACKSON, P. K. 2013. The Ciliary G-Protein-Coupled Receptor Gpr161 Negatively Regulates the Sonic Hedgehog Pathway via cAMP Signaling. *Cell,* 152**,** 210-223.

NAGATA, A., HAMAMOTO, A., HORIKAWA, M., YOSHIMURA, K., TAKEDA, S. & SAITO, Y. 2013. Characterization of ciliary targeting sequence of rat melanin-concentrating hormone receptor 1. *General and comparative endocrinology,* 188**,** 159-165.

NILSSON, S. E. 1964. Receptor Cell Outer Segment Development And Ultrastructure of the Disk Membranes in the Retina of the Tadpole (Rana Pipiens). *Journal of Ultrastructure Research,* 11**,** 581-602.

PALCZEWSKI, K., KUMASAKA, T., HORI, T., BEHNKE, C. A., MOTOSHIMA, H., FOX, B. A., LE TRONG, I., TELLER, D. C., OKADA, T., STENKAMP, R. E., YAMAMOTO, M. & MIYANO, M. 2000. Crystal structure of rhodopsin: A G protein-coupled receptor. *Science,* 289**,** 739-745.

PARK, J. H., SCHEERER, P., HOFMANN, K. P., CHOE, H.-W. & ERNST, O. P. 2008. Crystal structure of the ligand-free G-protein-coupled receptor opsin. *Nature,* 454**,** 183.

PEARRING, J. N., SALINAS, R. Y., BAKER, S. A. & ARSHAVSKY, V. Y. 2013. Protein sorting, targeting and trafficking in photoreceptor cells. *Progress in retinal and eye research,* 36**,** 24-51.

PEARRING, J. N., SAN AGUSTIN, J. T., LOBANOVA, E. S., GABRIEL, C. J., LIEU, E. C., MONIS, W. J., STUCK, M. W., STRITTMATTER, L., JABER, S. M. & ARSHAVSKY, V. Y. 2017. Loss of Arf4 causes severe degeneration of the exocrine pancreas but not cystic kidney disease or retinal degeneration. *PLoS genetics,* 13**,** e1006740.

PLOIER, B., CARO, L. N., MORIZUMI, T., PANDEY, K., PEARRING, J. N., GOREN, M. A., FINNEMANN, S. C., GRAUMANN, J., ARSHAVSKY, V. Y. & DITTMAN, J. S. 2016. Dimerization deficiency of enigmatic retinitis pigmentosa-linked rhodopsin mutants. *Nature Communications,* 7.

PUGH, E. & LAMB, T. 2000. Phototransduction in Vertebrate Rods and Cones:. *Handbook of Biological Physics.* Elsevier Science B. V. .

RÖHLICH, P. 1975. The sensory cilium of retinal rods is analogous to the transitional zone of motile cilia. *Cell and tissue research,* 161**,** 421-430.

SALINAS, R. Y., BAKER, S. A., GOSPE III, S. M. & ARSHAVSKY, V. Y. 2013. A single valine residue plays an essential role in peripherin/rds targeting to photoreceptor outer segments. *PLoS One,* 8**,** e54292.

SALINAS, R. Y., PEARRING, J. N., DING, J.-D., SPENCER, W. J., HAO, Y. & ARSHAVSKY, V. Y. 2017. Photoreceptor discs form through peripherin-dependent suppression of ciliary ectosome release. *J Cell Biol***,** jcb. 201608081.

SALOM, D., LODOWSKI, D. T., STENKAMP, R. E., LE TRONG, I., GOLCZAK, M., JASTRZEBSKA, B., HARRIS, T., BALLESTEROS, J. A. & PALCZEWSKI, K. 2006. Crystal structure of a photoactivated deprotonated intermediate of rhodopsin. *Proceedings of the National Academy of Sciences,* 103**,** 16123-16128.

STANDFUSS, J., EDWARDS, P. C., D'ANTONA, A., FRANSEN, M., XIE, G., OPRIAN, D. D. &

SCHERTLER, G. F. 2011. The structural basis of agonist-induced activation in constitutively active rhodopsin. *Nature,* 471**,** 656.

SUNG, C. H., DAVENPORT, C. M., HENNESSEY, J. C., MAUMENEE, I. H., JACOBSON, S. G., HECKENLIVELY, J. R., NOWAKOWSKI, R., FISHMAN, G., GOURAS, P. & NATHANS, J. 1991. Rhodopsin mutations in autosomal dominant retinitis pigmentosa. *Proc Natl Acad Sci U S A,* 88**,** 6481-6485.

SUNG, C. H., MAKINO, C., BAYLOR, D. & NATHANS, J. 1994. A rhodopsin gene mutation responsible for autosomal dominant retinitis pigmentosa results in a protein that is defective in localization to the photoreceptor outer segment. *J Neurosci,* 14**,** 5818-33.

TAI, A. W., CHUANG, J. Z., BODE, C., WOLFRUM, U. & SUNG, C. H. 1999. Rhodopsin's carboxy-terminal cytoplasmic tail acts as a membrane receptor for cytoplasmic dynein by binding to the dynein light chain Tctex-1. *Cell,* 97**,** 877-87.

TAM, B. M., MORITZ, O. L., HURD, L. B. & PAPERMASTER, D. S. 2000. Identification of an outer segment targeting signal in the COOH terminus of rhodopsin using transgenic Xenopus laevis. *The Journal of cell biology,* 151**,** 1369-1380.

TAM, B. M., MORITZ, O. L. & PAPERMASTER, D. S. 2004. The C terminus of peripherin/rds participates in rod outer segment targeting and alignment of disk incisures. *Molecular biology of the cell,* 15**,** 2027-2037.

TOKUYASU, K. & YAMADA, E. 1959. The fine structure of the retina studied with the electron microscope. IV. Morphogenesis of outer segments of retinal rods. *J Biophys Biochem Cytol,* 6**,** 225-30.

TSUJIKAWA, M. & MALICKI, J. 2004. Intraflagellar transport genes are essential for differentiation and survival of vertebrate sensory neurons. *Neuron,* 42**,** 703-16.

WANG, J., MORITA, Y., MAZELOVA, J. & DERETIC, D. 2012. The Arf GAP ASAP1 provides a platform to regulate Arf4 - and Rab11 – Rab8 - mediated ciliary receptor targeting. *The EMBO journal,* 31**,** 4057-4071.

YING, G., GERSTNER, C. D., FREDERICK, J. M., BOYE, S. L., HAUSWIRTH, W. W. & BAEHR, W. 2016. Small GTPases Rab8a and Rab11a are dispensable for rhodopsin transport in mouse photoreceptors. *PLoS One,* 11**,** e0161236.

YOUNG, R. W. 1967. The renewal of photoreceptor cell outer segments. *J Cell Biol,* 33**,** 61-72.

YOUNG, R. W. & DROZ, B. 1968. The renewal of protein in retinal rods and cones. *J Cell Biol,* 39**,** 169-84.

ZHANG, T., CAO, L.-H., KUMAR, S., ENEMCHUKWU, N. O., ZHANG, N., LAMBERT, A., ZHAO, X., JONES, A., WANG, S. & DENNIS, E. M. 2016. Dimerization of visual pigments in vivo. *Proceedings of the National Academy of Sciences,* 113**,** 9093-9098.

ZHAO, C. & MALICKI, J. 2011. Nephrocystins and MKS proteins interact with IFT particle and facilitate transport of selected ciliary cargos. *EMBO J,* 30**,** 2532-44.

Figures

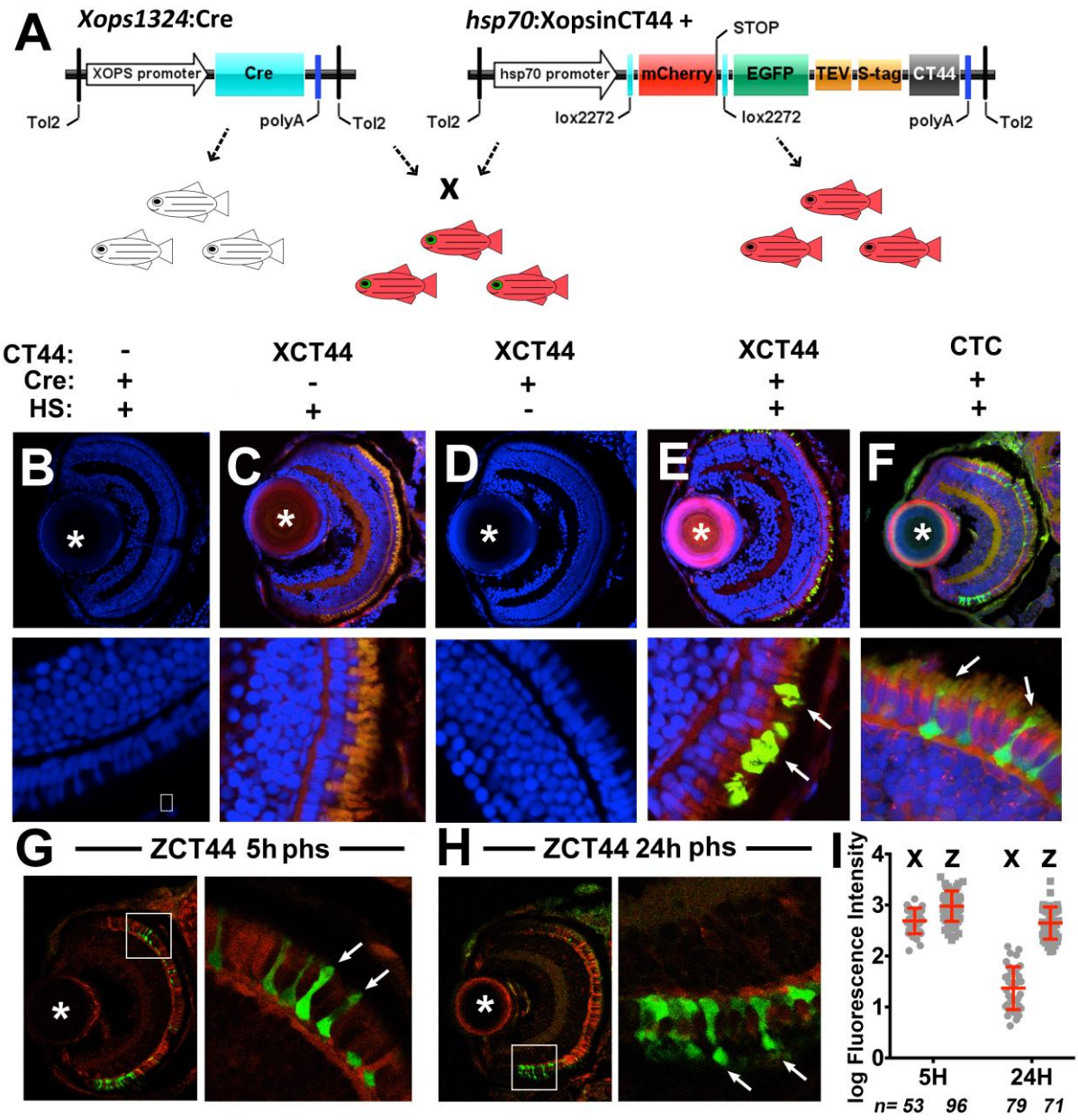

Fig. 1 (A) Schematic of transgenes used to obtain spatial and temporal control of expression for EGFP-S-opsinCT44 fusion proteins. (B-H) Confocal images of cryosections through the retinae of transgenic zebrafish larvae at 5 dpf. In (B-F), lower panels show higher magnification images. Transgene genotypes and heat shock treatment are indicated above. CTC, control random 44 amino acid peptide. (B) No fluorescent signal is observed in the Cre line even when heat shock is applied. (C) mCherry but not GFP expression is present when heat shock is applied to the hsp70:(mCherry)EGFP-S-opsinXCT44 transgenic line. (D) No fluorescent signal is observed in the double transgenic line when heat shock is not applied. (E)

EGFP is expressed in photoreceptors but not in other retinal cells when heat shock is applied to the double transgenic line containing Tg(XOPS-1324:Cre) and Tg(hsp70: lox2272-mCherry-lox2272-EGFP-2xTEV-S-tag-XCT44) transgenes. EGFP signal localizes to outer segments in this line (arrows in lower panels). (F) In contrast, EGFP signal remains in the cell body in a double transgenic line that contains a control EGFP construct in which CT44 cilia targeting signal was replaced with a random peptide. (G, H) High level of EGFP-S-opsinZCT44 persists in the photoreceptor cell body at 5 (G) and 12 (H) hours after heat shock. Panels to the right show enlargements of photoreceptors from images presented to the left. (I) GFP signal intensity in the cell body at 5h and 24h post heat shock for Xenopus (X) and zebrafish (Z) GFP-CT44 fusions. Log-transformed data from 2 independent experiments are shown. Each dot represents a measurement from a single photoreceptor cell. GFP is efficiently transported from the cell body to the outer segment when using the Xenopus but not the zebrafish CT44 ($p < 0.001$, ANOVA). In (B-F) sections are counterstained with DAPI (blue). Asterisks indicate the lens.

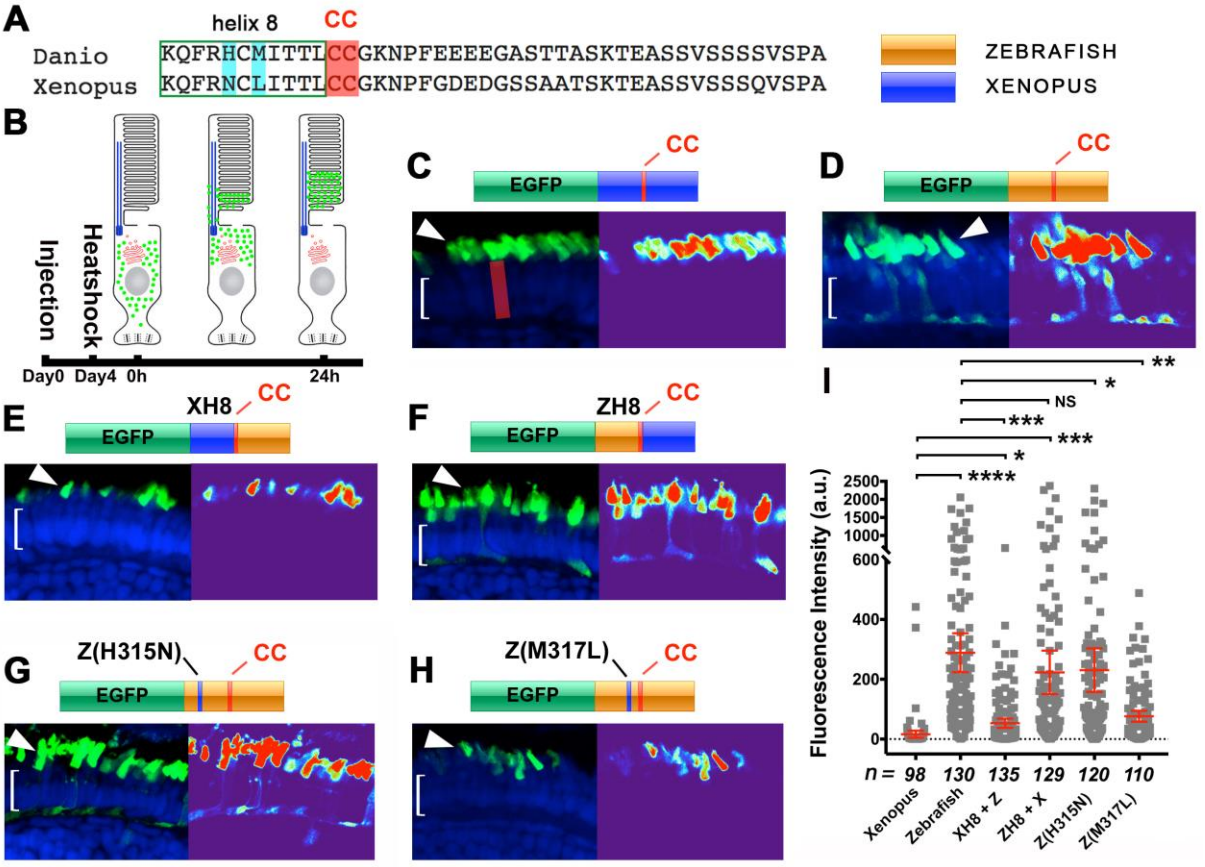

Fig. 2 Comparison of OS-targeting efficiency of Xenopus and zebrafish opsin C-terminal tails (CT44). (A) Alignment of rod opsin 44 C terminal amino acids from zebrafish and Xenopus. Palmitoylated cysteines are highlighted in red. (B) A schematic demonstrates the process of the transient assay. (C-H) Confocal images of cryosections through the photoreceptor cell layer of wild-type zebrafish retinae, that transiently express the following variants of the EGFP-CT44 construct at 5 dpf: (C) XCT44; (D) ZCT44; (E) ZCT H8 + X; (F) XCT H8 + Z; (G) Z-H315N; (H) Z-M317L. Confocal image (left) and a heat map (right) of GFP signal intensity are juxtaposed. Brackets indicate the photoreceptor cell layer, arrowheads point to outer segments. (I) Quantification of fluorescence intensity in photoreceptor cell bodies. The red rectangle in (C) approximately shows the soma of a single photoreceptor cell. Each dot represents a measurement from a single photoreceptor cell. Data are from 3 independent experiments. Mean and 95% confidence interval are indicated. Sample sizes are provided in italics below the horizontal axis. In schematic drawings above panels (C-H), zebrafish and Xenopus sequences are color-coded in orange and blue, respectively. Red bars indicate

conserved cysteine residues in opsin C terminus. Data are log transformed for statistical analysis as described in methods.

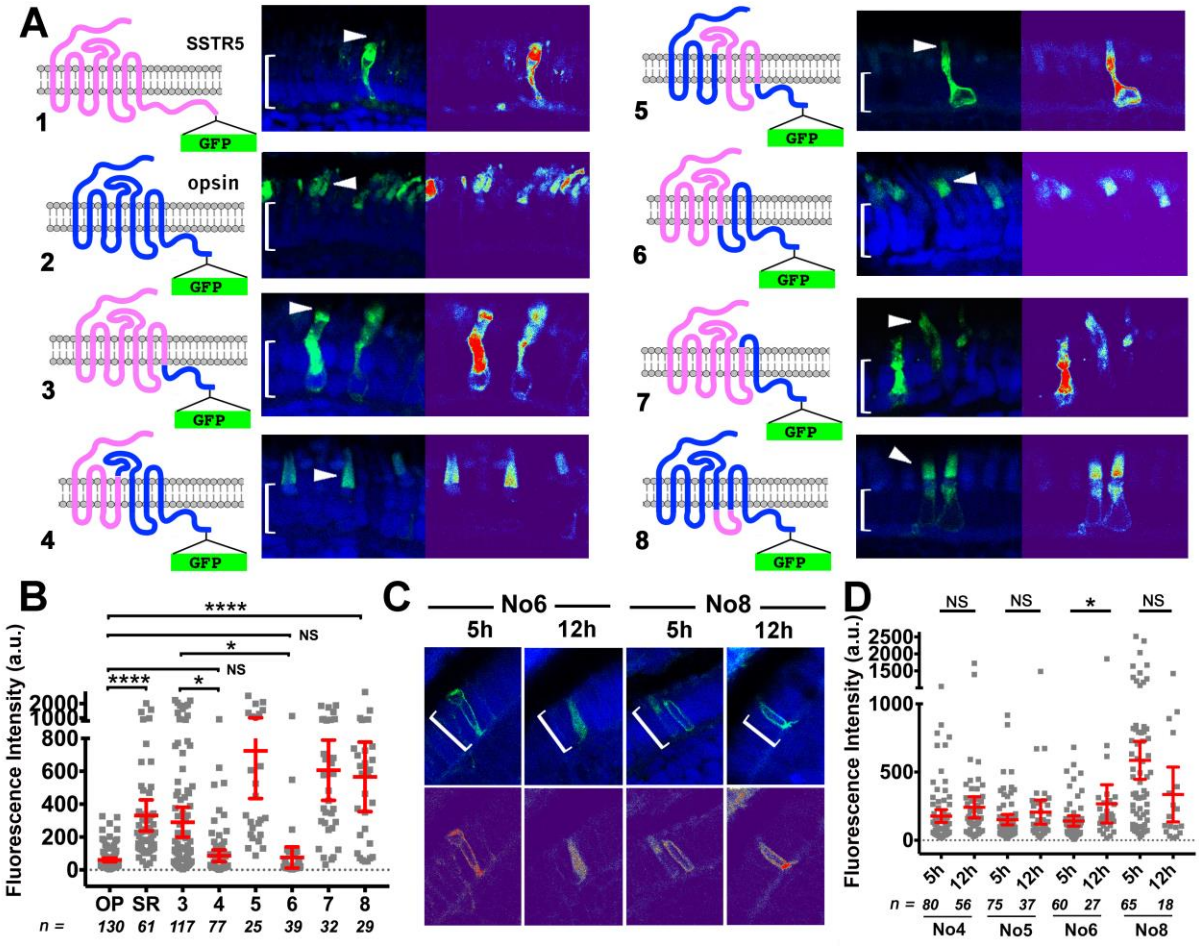

Fig.3 Transport efficiency of opsin/Sstr5 hybrid GPCRs into photoreceptor ciliary compartment**.** (A) Images of cryosections through zebrafish retinae expressing wild-type or hybrid GPCRs schematically shown to the left of each image. Brackets indicate the photoreceptor cell layer, arrowheads point to outer segments. In each panel, a confocal image (left) and a heat map (right) of GFP signal intensity are shown. (B) Quantification of the GFP signal intensity in photoreceptor cell bodies for wild-type and hybrid GPCRs shown in (A). Data from 4 independent experiments are provided. (C) Images of cryosections showing the expression of two hybrid GPCRs in *oval*$^{-/-}$ mutant photoreceptors at 5 and 12 h post heat shock as indicated in above panels. A confocal image (top) and a heat map (bottom) of GFP signal intensity are shown. (D) Quantification of GFP signal intensity in the cell bodies of *oval*$^{-/-}$

mutant photoreceptors expressing 4 hybrid GPCRs at 5 and 12 h post heat shock as indicated. Data are from 4 independent experiments. In (B, D) each dot represents a single photoreceptor, mean and 95% confidence interval are provided, sample sizes are in italics below the horizontal axis.

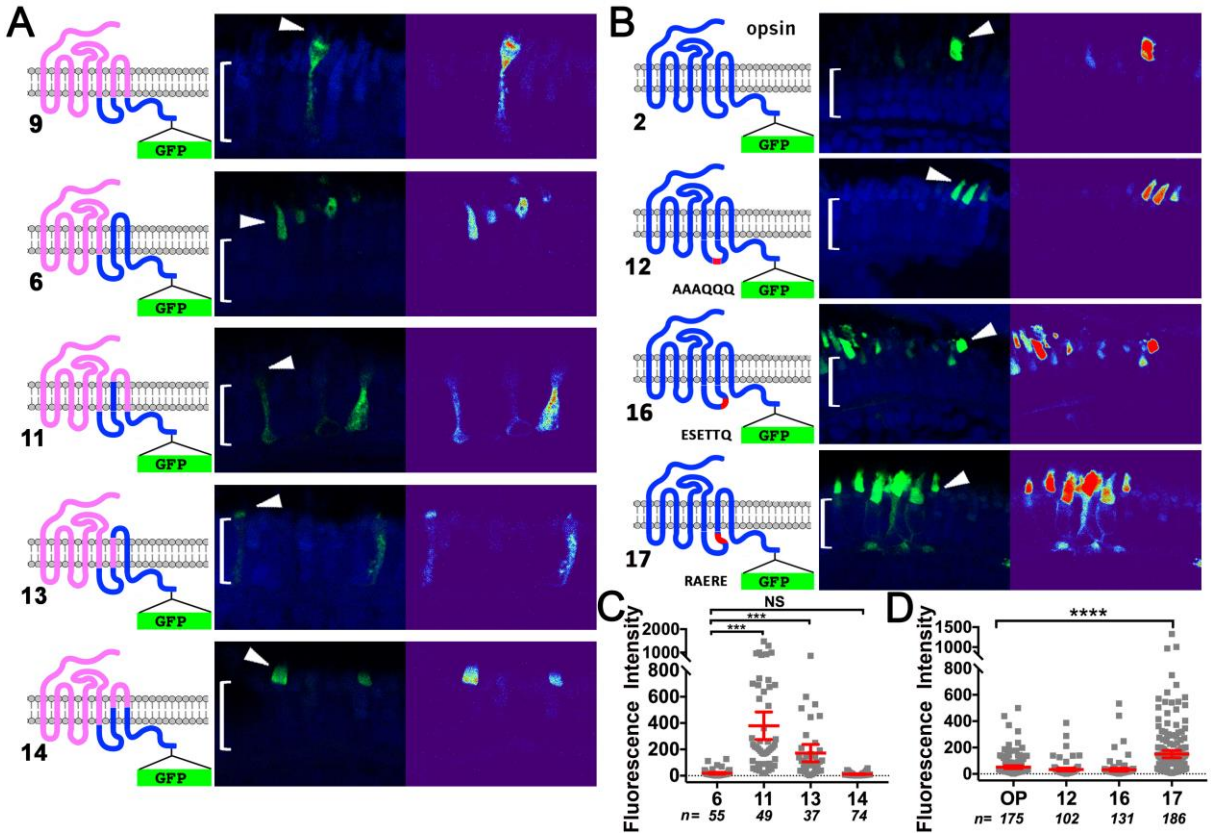

Fig. 4 Transport efficiency of opsin/Sstr5 hybrid GPCRs (continued from Fig. 3). (A, B) Images of cryosections through zebrafish retinae expressing wild-type or hybrid GPCRs schematically shown to the left of each image. Brackets indicate the photoreceptor cell layer, arrowheads point to outer segments. In each panel, a confocal image (left) and a heat map (right) of GFP signal intensity are shown. (C) Quantification of the GFP signal intensity in photoreceptor cell bodies for hybrid GPCRs shown in (A). (D) Quantification of the GFP signal intensity in photoreceptor cell bodies for hybrid GPCRs shown in (B). In (C, D), data originate from 3 independent experiments, each dot represents a single photoreceptor, mean and 95% confidence interval are shown, sample sizes are in italics below the horizontal axis.

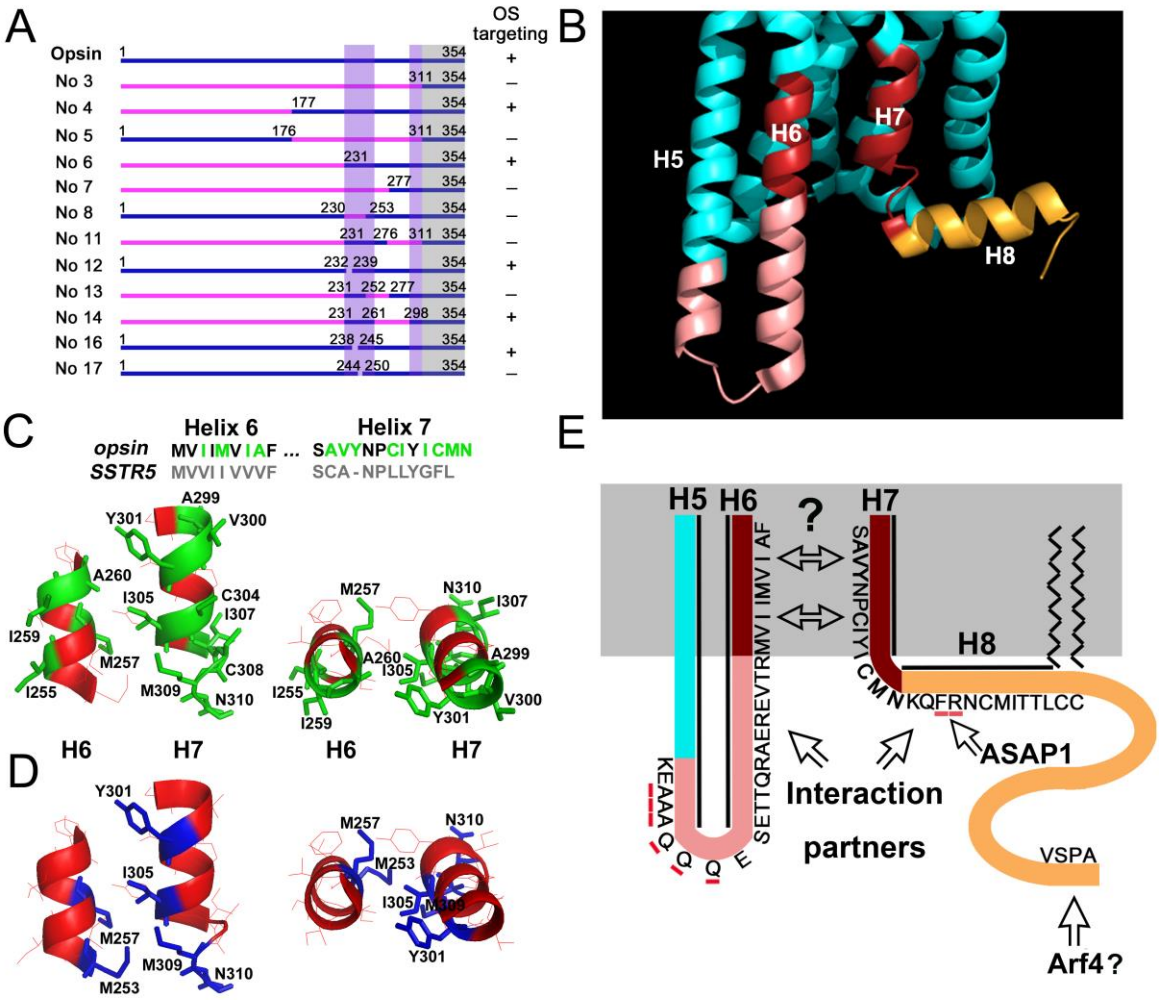

772

773 **Fig. 5** Summary of opsin OS targeting motifs identified in this and previous studies. (A)
774 Summary of results from Figs. 3 and 4. Rod opsin sequences included in each construct are
775 represented as blue horizontal bars, Sstr5 sequences are depicted in pink. The first and the
776 last amino acid of each opsin fragment are numbered. Sequences necessary for the ciliary
777 targeting of opsin are highlighted by vertical bars. The CT44 is indicated by a grey vertical
778 bar. (B) The structure of opsin monomer based on X-ray crystallography (PDB: 3CAP).
779 Fragments of transmembrane helixes near the cytoplasmic face of the membrane and
780 cytoplasmic loops are shown. Helix 8 is highlighted in orange, IC3 is in pink, and the portions
781 of helix 6 and 7 that we found necessary for opsin transport are red. The remaining sequences
782 are in cyan. (C, D) Regions of helix 6 and 7 necessary for opsin transport in side view and
783 viewed along helix axis. (C) Amino acid side chains that differ between zebrafish rod opsin
784 and zebrafish Sstr5 are numbered and depicted in green. (D) Amino acids that are conserved

785 in ciliary but not in rhabdomeric opsins are numbered and depicted in blue. (E) Schematic
786 representation of opsin features that are necessary and sufficient for the ciliary targeting of
787 opsin. Sequences are color coded as in (B). Helixes are indicated with solid black lines.
788 The SSTR3 ciliary targeting motif and the FR motif are underlined in red. Arrows indicate
789 potential interaction sites with proteins that facilitate opsin transport based on work of several
790 groups. In (C, D), two amino acid substitutions were made: $V_{Bos}304$ to C_{Danio} and $V_{Bos}308$ to
791 C_{Danio} to match the zebrafish sequence. In (B-D), protein structure is visualized using PyMOL
792 software.